Molecular Physics, Vol. 103, Nos. 21–23, 10 November–10 December 2005, 3103–3113

Freezing and melting of azeotropic mixtures confined in nanopores: experiment and molecular simulation

J. CZWARTOS†, B. COASNE‡§, K. E. GUBBINS*‡, F. R. HUNG‡
and M. SLIWINSKA-BARTKOWIAK†

†Institute of Physics, Adam Mickiewicz University, Umultowska 85, 61-614 Poznan, Poland
‡Department of Chemical and Biomolecular Engineering, North Carolina State University, Raleigh, NC 27695-7905, USA
§Laboratoire de Physicochimie de la Matière Condensée, CNRS (UMR 5617) & Université de Montpellier II, Place Eugène Bataillon, 34095 Montpellier Cedex 05, France

(*Received 20 April 2005; accepted 1 June 2005*)

The paper reports on a qualitative comparison between experimental measurements and molecular simulations of the freezing and melting of azeotropic mixtures confined in nanoporous materials. Dielectric relaxation spectroscopy was used to determine the experimental solid/liquid phase diagram of CCl_4/C_6H_{12} mixtures confined in activated carbon fibres. Grand Canonical Monte Carlo simulations combined with the parallel tempering technique were used to model the freezing of the azeotropic Lennard–Jones mixture Ar/CH_4 in a graphite slit pore. The structure of the crystal phase in the simulations is investigated by means of positional and bond-orientational pair correlation functions and appropriate bond-order parameters. Both simulations and experiments show that the phase diagram of the confined mixture is of the same type as that for the bulk, but the solid/liquid coexistence lines are located at higher temperatures. The effect of confinement and of the wall/fluid interaction on the location of the azeotrope is discussed.

1. Introduction

Freezing and melting of fluids in nanoporous materials are of particular interest for the understanding of thermodynamics of phase transitions in confined geometry and for many applications that involve confined systems (lubricating properties of thin films in nanotechnologies, preparation of nanostructures, phase separation processes, distribution of pollutants in soils, etc.). Many experimental and molecular simulation studies have focused on the freezing and melting of pure fluids confined in various nanoporous materials (for reviews see [1–3]). Only a few studies have been reported for the freezing of confined binary systems, such as molten salts [4, 5] and colloidal mixtures [6]; the transition temperature and the density of the system were found to be significantly different from the bulk. Recently, the authors studied, by means of molecular simulations, the confinement effect on the solid/liquid phase diagram of Lennard–Jones Ar/Kr mixtures confined in slit pores [7, 8]. It was shown that the phase diagram for the confined mixture is of the same type as that for the bulk, i.e. ideal solution. In agreement with previous molecular simulations and experiments for pure fluids [1–3], it was also found that the freezing temperature of the confined mixture is lower or larger than the bulk, depending on the ratio of wall–fluid to fluid–fluid interactions [7, 8].

In this paper, we extend our previous studies by considering the freezing and melting of binary mixtures having an azeotropic phase diagram. We report experiments and molecular simulations for azeotropic mixtures confined in slit graphite pores. In each case, the solid/liquid phase diagram of the mixture was determined for both the bulk and the confined system in order to estimate the effect of confinement on the melting temperature and the location of the azeotrope. The experimental measurements consist of dielectric relaxation spectroscopy for CCl_4/C_6H_{12} confined in activated carbon fibres of pore width 1.2 nm, corresponding to a reduced pore width $H^* = H/\sigma \sim 2.4$ (σ is the size of the adsorbate, $\sigma_{CCl_4} = 0.514$ nm and $\sigma_{C_6H_{12}} = 0.500$ nm [9]). The molecular simulations were performed for an azeotrope Lennard–Jones Ar/CH_4 mixture confined within a slit pore having a similar

*Corresponding author. Email: keg@ncsu.edu

Molecular Physics
ISSN 0026–8976 print/ISSN 1362–3028 online
http://www.tandf.co.uk/journals
DOI: 10.1080/00268970500200101

reduced pore width, $H^* \sim 2.7\sigma_{CH_4}$ ($\sim 3\sigma_{Ar}$), to that considered in the experiments. The phase diagram of the bulk and confined mixtures were determined using the Gibbs–Duhem integration technique [10–14] and Grand Canonical Monte Carlo simulations [15–17], respectively. Following previous works on the freezing of pure substances [9, 18], we analyse our results in terms of the parameter α, defined as the ratio of the wall/fluid to the fluid/fluid attractive interactions. We also discuss the structure of the confined phase by calculating in the simulations 2D bond-order parameters and both 2D in-plane positional and bond-orientational pair correlation functions.

The paper is organized as follows. In section 2, we present details of the experimental and molecular simulation techniques. In section 3, we first discuss our experimental results obtained for melting of CCl_4/C_6H_{12} mixtures confined in activated carbon fibers. Then, we present data obtained from molecular simulations of freezing of Ar/CH_4 confined in a slit graphite pore. In section 4, we summarize our results and suggest future works. We are pleased to contribute this paper in honor of Benjamin Widom on the occasion of this special issue of *Molecular Physics*. Among his numerous scientific works, Widom made significant contributions to the field of molecular simulation and theory of surface thermodynamics (adsorption, hydrophobicity, surface tension, etc.) [19–25].

2. Methods

2.1. *Experiment*

Activated carbon fibres (ACF) having a mean pore width of 1.2 nm were used in this work to study the freezing upon confinement of CCl_4/C_6H_{12} mixtures. Pores in this material, which are approximately of a slit-shape geometry, are expected to accommodate two layers of CCl_4 or C_6H_{12} since the reduced pore width is $H^* \sim 2.4$ (using either the size of CCl_4 or C_6H_{12}) [9, 26]. CCl_4 and C_6H_{12} were distilled twice prior to their use in experiments. Sodium was added to the solution in the case of C_6H_{12} to trap water molecules. Samples were outgassed over 5 days at a temperature of 150°C and under a vacuum of 10^{-4} Torr, prior to introduction of the mixture. Dielectric relaxation spectroscopy (DRS) of the confined mixture was performed using a parallel plate capacitor of empty capacitance $C_0 = 69.1$ pF. The capacitance C and the tangent loss tan δ (where δ is the angle by which current leads the voltage) of the filled sample were measured at different temperatures using a SI 1260 impedance/gain phase analyser in the frequency range 10 Hz–10 MHz. The real and imaginary parts of the complex dielectric permittivity $\varepsilon^* = \varepsilon' - i\varepsilon''$ are related to the capacitance and tangent loss of the system, $\varepsilon' = C/C_0$ and $\varepsilon'' = \tan(\delta)/\varepsilon'$ [27, 28]. A schematic view of the experimental setup is shown in figure 1.

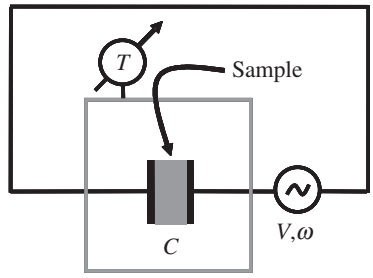

Figure 1. Schematic view of the experimental setup used in dielectric relaxation spectroscopy. A suspension of filled ACF in the bulk mixture is introduced between the parallel plates of a capacitor having a capacitance of $C_0 = 69.1$ pF when empty. The melting of the system is determined by monitoring as a function of temperature T the response (permittivity) of the confined mixture upon an electric field (voltage V) oscillating at a frequency ω.

Melting of a solid phase can be monitored in the DRS experiment by a large increase of the permittivity. The sample was introduced between the capacitor plates (covered by a teflon layer) as a suspension of ACF filled with the mixture in the bulk mixture. Therefore, the measurements yield an effective permittivity that has contributions from the bulk and the confined mixtures. During the experiments, the temperature of the sample was controlled with an accuracy of 0.1 K using a cryostat.

2.2. *Molecular simulation*

2.2.1. Phase diagram of the bulk mixture: Gibbs–Duhem integration. Following previous work by Lamm and Hall on the freezing of bulk mixtures [29–31], we determined the solid–liquid phase diagram of the bulk Lennard–Jones Ar/CH_4 mixture using the Gibbs–Duhem integration technique (GDI) [10–12, 32]. This method has been shown to reproduce correctly the shape of the experimental phase diagram for several mixtures [29–31]. The GDI technique consists of determining the phase coexistence line by integrating the Clapeyron equation. For the binary mixtures AB, the Clapeyron equation describing the coexistence at constant pressure between the solid (s) and the liquid (l) phases is [14, 32]:

$$\frac{d\beta}{d\xi_B} = \frac{\left(x_B^l - x_B^s\right)}{\xi_B(1-\xi_B)\left(h_B^l - h_B^s\right)}, \tag{1}$$

where $\beta = 1/kT$ is the reciprocal temperature, ξ_B is the fugacity fraction of component B. x_B and h_B are the

mole fraction and the enthalpy of component B, respectively. In the GDI method, equation (1) is integrated in order to find the relation $\beta(\xi_B)$ that describes the solid/liquid coexistence when the fugacity fraction ξ_B varies from 0 to 1. The initial conditions of the integration procedure are given by considering the slope of equation (1) at infinite dilution of B when pure fluid A is at the solid/liquid coexistence conditions. At each integration step $\beta(\xi_B)$, Monte Carlo simulations in the semi-grand canonical $NPT\xi_B$ are performed for both the liquid and solid phases in order to estimate the enthalpies, h_B^l and h_B^s, and the mole fractions, x_B^l and x_B^s. This set of two simulations is repeated using a predictor–corrector method until the integrand in equation (1) converges. The solid/liquid phase diagram (T, x_B) at constant pressure P of the mixture can be built by reporting at each reciprocal temperature β the mole fraction of the solid and liquid phases, i.e. x_B^l and x_B^s.

NPT ξ_B Monte Carlo simulations were performed at a pressure $P = 1$ atm for $N = 500$ particles contained in a cubic box with periodic boundary conditions. Moves in the semi-grand canonical ensemble (particle displacement, volume change, and particle exchange) were attempted randomly and accepted according to the following acceptance probability:

$$P_{acc} = \min\left\{1,\ \exp\left[(-\beta(U_N - U_O) - \beta P(V_N - V_O) + N\ln\frac{V_N}{V_O} + \lambda_{AB}\ln\frac{\xi_B}{1-\xi_B}\right]\right\}, \quad (2)$$

where U_N and U_O, and V_N and V_O are the energies and volumes of the configuration after and before the move. λ_{AB} equals 1 if the particle exchange attempt is from A to B and equals -1 if the particle exchange attempt is from B to A. The interactions Ar/Ar and CH_4/CH_4 were calculated using Lennard–Jones potentials with the following parameters [33]: $\sigma_{Ar/Ar} = 3.405$ Å, $\varepsilon_{Ar/Ar}/k = 119.8$ K, and $\sigma_{CH_4/CH_4} = 3.810$ Å, $\varepsilon_{CH_4/CH_4}/k = 148.1$ K. The cross-species Ar/CH_4 parameters were calculated using the Lorentz–Berthelot combining rules [34]. The Lennard–Jones potentials were truncated at a distance of half the size of the simulation box and long-range correction to the energy was used [16]. The GDI and $NPT\xi_B$ Monte Carlo algorithms used in this work are similar to those developed by Lamm and Hall; full details regarding these techniques can be found elsewhere [13, 14, 29–31].

2.2.2. Phase diagram of the confined mixture: Grand Canonical Monte Carlo simulations. The solid–liquid phase diagram at $P = 1$ atm of the Ar/CH_4 mixture confined in graphite slit pores was determined using the Grand Canonical Monte Carlo technique (GCMC). This stochastic method simulates a system having a constant volume V (the pore with the adsorbed phase), in equilibrium with an infinite fictitious reservoir of particles imposing its chemical potential for each species, μ_A and μ_B, and its temperature T [15–17]. Particle displacement, insertion, and deletion were attempted randomly. The sampling of the phase space was improved by adding a fourth move that consists of exchanging the identity of an existing particle [35]. In order to circumvent the difficulty of particle deletion and insertion in dense phases such as liquids and solids, we combined the GCMC simulations with the parallel tempering technique [17, 36, 37]. This method consists of considering several replicas of the system at different temperatures and chemical potentials. In addition to conventional Monte Carlo moves that are performed for each replica, trial swap moves between configurations in different replicas are attempted. The parallel tempering technique prevents the system from being 'trapped' in local metastable states [7, 8, 38–41]. Full details of the technique of the GCMC and parallel tempering techniques used in this work have been described elsewhere [7].

We studied the freezing of Ar/CH_4 mixtures confined in a graphite slit pore of a width 1.02 nm, i.e. $H \sim 2.7\sigma_{CH_4/CH_4} \sim 3\sigma_{Ar/Ar}$. The size of the square section was 22.9 nm × 22.9 nm ($\sim 60\sigma_{CH_4/CH_4} \times 60\sigma_{CH_4/CH_4}$). Periodic boundary conditions were applied in the directions (x, y) parallel to the pore walls. As in the case of the bulk mixture (see section 2.2.1), the fluid/fluid interactions Ar/Ar, CH_4/CH_4, and Ar/CH_4 were calculated using Lennard–Jones potentials. The slit graphite pore was described as an assembly of two structureless parallel walls. The interaction between the fluid and each pore wall was calculated using the Steele '10–4–3' potential [42, 43]:

$$U_{wf}(z) = 2\pi\rho_w\varepsilon_{wf}\sigma^2\Delta\left[\frac{2}{5}\left(\frac{\sigma_{wf}}{z}\right)^{10} - \left(\frac{\sigma_{wf}}{z}\right)^4 - \left(\frac{\sigma_{wf}^4}{3\Delta(z+0.61\Delta)^3}\right)\right], \quad (3)$$

where z is the distance between the adsorbed molecule and the graphite surface. Δ is the separation between graphite layers, 0.335 nm, and ρ_w the atomic density of graphite layers, 114 nm^{-3}. The wall/fluid Lennard–Jones parameters $\varepsilon_{w/Ar}$, $\sigma_{w/Ar}$, ε_{w/CH_4}, and σ_{w/CH_4} were determined by combining the wall/wall and fluid/fluid parameters using the Lorentz–Berthelot rules with the values $\varepsilon_{ww}/k_B = 28$ K and $\sigma_{ww} = 0.34$ nm for the carbon

Table 1. Parameters α for the different mixture components studied in this work (experiment and molecular simulation). α is defined as the ratio of the wall/fluid to the fluid/fluid attractive interactions (see section 2.2.2). In the case of the experimental system, ACFs were modeled as graphite slit pores and the mixture components as Lennard–Jones fluids (see text).

(Experiment)	CCl_4	$\alpha = 1.93$
	C_6H_{12}	$\alpha = 1.76$
(Simulation)	Ar	$\alpha = 2.14$
	CH_4	$\alpha = 2.16$

wall [43]. Radhakrishnan *et al*. [9, 18] have shown that the parameter $\alpha = \rho_w \varepsilon_{wf} \sigma_{wf}^2 \Delta / \varepsilon_{ff}$, i.e. the ratio of the wall/fluid to the fluid/fluid attractive interactions, can be used to describe the change in freezing temperature of a confined system. An increase (decrease) in the freezing temperature compared to the bulk is expected for $\alpha > 1$ ($\alpha > 1$). The α parameters for Ar and CH_4 confined in graphite pore are shown in table 1. We also report in table 1 the α parameters for CCl_4 and C_6H_{12} confined in activated graphite pores, which corresponds to the system considered in the experiments; α was estimated using equation (3) i.e. ACF pores were modeled as graphite slit pores and the mixture components as Lennard–Jones fluids. In both the experimental and molecular simulation studies, the α parameters are greater than 1 for all components, so that we expect the freezing temperature of the confined mixtures to be larger than that of the bulk.

The input parameters required in the GCMC simulations, $\mu_{Ar}(T)$ and $\mu_{CH_4}(T)$ at constant pressure $P = 1$ atm, were determined using the equation of state for Lennard–Jones mixtures of Johnson *et al*. [44]. The number of particles in our simulations varies from 5000–8000, depending on the mole fraction of the confined mixture. The number of replicas used in this work is 16 and the temperature difference between two successive replicas is $\Delta T = 2$ or 3 K. We started with well equilibrated liquid configurations of the confined mixture and performed, at least, 10^5 Monte Carlo steps per particle to equilibrate the system using the parallel tempering technique. After equilibration of the system, density profiles, bond order parameters, and pair correlation functions were averaged in the course of a second simulation run.

Strong layering was observed due to the interaction with the attractive pore walls. Following previous work on freezing of pure fluids in nanopores [9, 40, 41, 45, 46], the structure of the confined mixture was investigated by calculating for each layer i the 2D bond-order parameters $\alpha_{6,i}$. We determined $\alpha_{6,i}$ as the average value of the local order parameter $\Psi_{6,i}(\mathbf{r})$, which measures the hexagonal bond-order at a position $\mathbf{r}$ of a particle located in the layer i [47, 48]:

$$\Psi_{6,j}(\mathbf{r}) = \frac{1}{N_b} \sum_{k=1}^{N_b} \exp(i6\theta_k) \quad \text{with} \quad \Phi_{6,j} = \frac{\left| \int \Psi_{6,j}(\mathbf{r}) d\mathbf{r} \right|}{d\mathbf{r}} \tag{4}$$

Where θ_k are the bond angles between the particle and each of its N_b nearest neighbors. $\Phi_{6,i}$ is close to 1 for a crystal layer having a triangular structure and close to 0 for a liquid layer. We also monitored the 2D in-plane positional and bond-orientational pair correlation functions, $g_i(\mathbf{r})$ and $G_{6,i}(\mathbf{r})$ [7, 9, 18, 46, 49]. The latter measures for each layer i the correlations between the local bond order parameter $\Psi_{6,j}(\mathbf{r})$ at two positions separated by a distance $\mathbf{r}$:

$$G_6(\mathbf{r}) = \left\langle \Psi_{6,j}^*(0) \Psi_{6,j}(\mathbf{r}) \right\rangle \tag{5}$$

3. Results and discussion

3.1. *Experiment*

Measurements of the dielectric constant $\varepsilon' = C/C_0$ allow the investigation of melting phenomena, as the polarizability of the liquid and solid phases are significantly different [27]. A change in the slope of the capacitance versus temperature curve shows that melting occurs in the system. Upon melting of a mixture (bulk or confined), this change occurs at the temperature of the solidus point (i.e. when the crystal starts melting), while the temperature where the linearity of the function $C(T)$ is observed again corresponds to the liquidus point (corresponding to the temperature where the whole crystal has melted). The capacitance curve C as a function of the temperature T is shown in figure 2 for a CCl_4/C_6H_{12} mixture with $x_{C_6H_{12}} = 0.4$ confined at a constant pressure $P = 1$ atm in ACF with a pore width $H = 1.2$ nm. Melting for both the bulk and the confined mixtures is observed as the sample consists of a suspension of filled ACF in the bulk mixture (see section 2.1). A first large increase in the capacitance is observed at $T = -25.0^\circ$C; this corresponds to the melting temperature of the bulk mixture for $x_{C_6H_{12}} = 0.4$. Such a result was checked by repeating these experiments for the bulk mixture only, i.e. without suspension of ACF. The increase in the capacitance at $T = -25.0^\circ$C indicates that the bulk crystal mixture starts melting i.e. the system reaches the crystal coexistence line. At $T = -23.3^\circ$C, the transformation of the bulk crystal into the liquid mixture is complete, i.e. the system

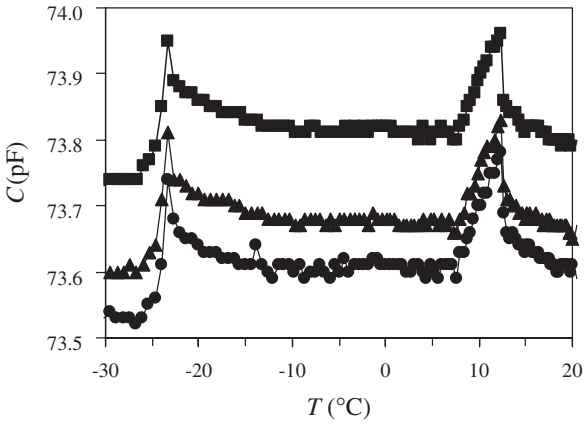

Figure 2. Capacitance C as a function of temperature T for a CCl_4/C_6H_{12} mixture with $x_{C_6H_{12}} = 0.4$ confined in ACF with a pore width $H = 1.2$ nm. The measurements were performed at constant pressure $P = 1$ atm for three different frequencies: (circles) $\omega = 100$ kHz, (triangles) $\omega = 600$ kHz, and (squares) $\omega = 1$ MHz. The signal is for both the bulk and confined mixtures since the sample consists of a suspension of filled ACF in the bulk mixture.

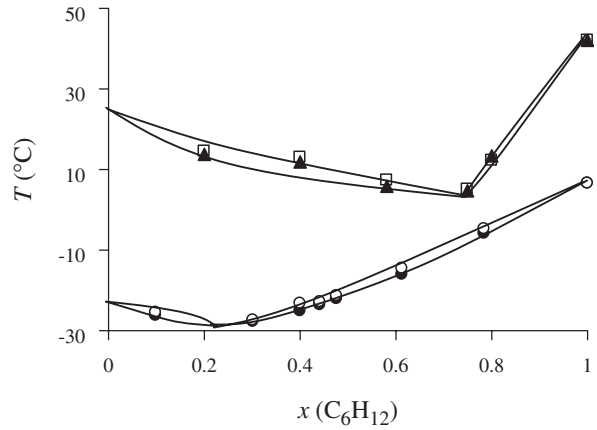

Figure 3. Solid/liquid phase diagram ($T, x_{C_6H_{12}}$) at constant pressure $P = 1$ atm for CCl_4/C_6H_{12}: (circles) are for the bulk mixture, and (triangles and squares) are for the mixture confined in ACF with a pore width $H = 1.2$ nm. Open and closed symbols denote the liquid and solid coexistence lines, respectively. The point for pure CCl_4 confined in ACF $H = 1.2$ nm was taken from [26]. The lines between the symbols are provided as a guide to the eye.

reaches the liquid coexistence line, and the capacitance of the system decreases as expected for a liquid phase [27, 28]. This analysis provides both the liquid and crystal coexistence temperatures for bulk CCl_4/C_6H_{12} mixture having a molar composition $x_{C_6H_{12}} = 0.4$. At a much higher temperature, $T = 12°C$, a second increase in the capacitance of the system is observed. The sudden change at this temperature, which does not correspond to any known transition temperature for a bulk CCl_4/C_6H_{12} mixture with $x_{C_6H_{12}} = 0.4$, is believed to represent the melting of the material confined within the ACF. As in the case of the bulk mixture, the crystal and liquid coexistence temperatures for this molar composition were estimated from the temperatures where the capacitance starts increasing and where the capacitance reaches a maximum, respectively, i.e. $T = 8°C$ and $T = 12°C$.

The experimental process described above was repeated for different mole fractions in order to obtain the solid/liquid phase diagram for confined CCl_4/C_6H_{12} mixtures. For a few molar compositions, the capacitance change upon melting consists of a change in the slope of the signal rather than a peak. It is believed that the nature of the change depends on the amounts of bulk and confined fluid in the sample, since the signal is the sum of the two contributions. For mixtures, we also expect the shape of the signal to depend on the mole fraction of the system. The phase diagram for CCl_4/C_6H_{12} within ACF having a pore width $H = 1.2$ nm is compared with that for the bulk in figure 3. The phase diagrams for the confined mixture and the bulk are of the same type, i.e. azeotrope, but the solid/liquid coexistence lines are located at higher temperature. The shift in the coexistence conditions is consistent with previous simulation, theoretical and experimental studies for pure fluids or mixtures, which have shown that the freezing temperature for systems confined in strongly attractive pores, i.e. α larger than 1, is increased compared to the bulk [7, 9, 18, 46, 50–52]. The relative increase in the freezing temperature is $T_f/T_{f,\text{bulk}} \sim 1.19$ for pure CCl_4 and $T_f/T_{f,\text{bulk}} \sim 1.12$ for pure C_6H_{12}. The larger shift for CCl_4 can be qualitatively explained by the larger α parameter for this fluid (see table 1). The increase in the freezing temperature $T_f/T_{f,\text{bulk}}$ as a function of $x_{C_6H_{12}}$ cannot be discussed quantitatively from our experiments since only the global mole fraction, i.e. the mole fraction of the whole sample (bulk and confined mixtures) introduced in the capacitor is known.

The location of the azeotrope for the confined mixture, $x_{0,C_6H_{12}} \sim 0.75$, is located at a global C_6H_{12} mole fraction larger than that for the bulk, $x_{0,C_6H_{12}} \sim 0.23$. Again, the interpretation of such a result remains difficult, as the mole fraction of the confined mixture is not known. However, we know from previous molecular simulations [7, 35] and theoretical calculations [53] that the mole fraction within the pore is shifted, compared to the bulk, towards the component having the strongest interaction with the pore walls (this departs from the qualitative change in freezing temperature, which is rather related to the α parameter). Given that the wall/fluid interaction is larger for C_6H_{12} than for CCl_4, we expect the C_6H_{12} mole fraction within the pore to be larger than that of the bulk. In other words,

the phase diagram shown in figure 3 for the confined mixture probably indicates C_6H_{12} mole fractions that underestimate the composition of the mixture in ACF. This shows that there is no straightforward analysis of the experimental results without knowing the mole fraction for the confined mixture. In order to complement our experimental investigation, we report in the following section a molecular simulation study for another azeotrope mixture confined in a graphite pore.

3.2. *Molecular simulation*

In this section, we report GCMC simulations for Ar/CH_4 mixtures confined in a graphite slit-pore having a width of 1.02 nm ($H = 2.7\sigma_{CH_4} = 3\sigma_{Ar}$). Each simulation run consisted of GCMC simulations with parallel tempering between 16 replicas at different temperature T_i but the same pressure $P = 1$ atm. In each run, the chemical potentials $\mu_{Ar}(T, P)$ and $\mu_{CH_4}(T, P)$ for each replica were calculated so that the confined mixture is in equilibrium with a bulk mixture having the same molar composition, $x^{bulk}_{CH_4}$. These conditions for the simulations correspond to the experimental process in which the confined mixture is at all temperatures in equilibrium with a bulk mixture having the same mole fraction (see section 3.1). The different runs performed in this work are summarized in table 2. Here we present, as an example, a detailed analysis of the results obtained for the run 2, i.e. where the confined mixtures are in equilibrium with a bulk Ar/CH_4 mixture having a mole fraction $x^{bulk}_{CH_4} = 0.50$. The complete solid/liquid phase diagram (T, x_{CH_4}) obtained from the analysis of the different runs will be discussed at the end of this section.

Table 2. Simulation runs performed in this work. A simulation run consists of GCMC simulations with parallel tempering between 16 replicas at different temperature but the same pressure $P = 1$ atm. Each of the 16 replicas is in equilibrium with a bulk mixture having the same molar composition, $x^{bulk}_{CH_4}$. For each run, the mole fraction of the bulk mixture is reported in the second column. The reduced freezing temperature for the confined mixture, T^*_f, is shown in the third column. $x^C_{CH_4}$ and $x^L_{CH_4}$ are the CH_4 mole fractions of the solid and liquid coexisting phases at the freezing temperature, respectively. The uncertainty is ±0.02 K for the freezing temperature and ±0.01 for the mole fractions. Bold data are results corresponding to the detailed analysis given in section 3.2.

Run	$x^{bulk}_{CH_4}$	T^*_f	$x^C_{CH_4}$	$x^L_{CH_4}$
1	1.00	1.32	1.00	1.00
2	**0.50**	**1.22**	**0.87**	**0.85**
3	0.20	1.14	0.66	0.64
4	0.10	1.09	0.51	0.49
5	0.05	1.05	0.36	0.34
6	0.02	1.05	0.20	0.20
7	0.01	1.05	0.11	0.12
8	0.00	1.05	0.00	0.00

For all molar compositions studied in this work, we found that the CH_4 mole fraction for the confined mixture is always larger than that of the bulk mixture. As shown in previous work [7, 35, 53], this result is due to the fact that CH_4 has a stronger interaction with the pore wall than Ar. Density profiles $\rho(Z^*)$ of the confined Ar/CH_4 mixture are shown in figure 4 for two different temperatures, $T^* = 1.14$ and $T^* = 1.36$ (temperatures are reduced with respect to ε_{Ar}). Z^* is the distance from the center of the slit pore in reduced units with respect to the Lennard–Jones parameter σ_{Ar}. The confined mixture has a layered structure, composed of two symmetrical layers directly in contact with the pore wall. By analyzing the different contributions $\rho_{Ar}(Z^*)$ and $\rho_{CH_4}(Z^*)$ (not shown), it was found that the ratio of the peak amplitude to the peak width is larger for CH_4 than that for Ar. This result shows that, due to their larger size, CH_4 molecules are more localized than Ar atoms [7].

The average value of the 2D bond-order parameter for the confined layers, Φ_6, is shown in figure 5 as a function of the temperature. Upon freezing, Φ_6 sharply increases at $T^* \sim 1.22$, which reveals that the confined layers undergo a liquid to crystal phase transition. Φ_6 varies from ~0.03 in the liquid region up to ~0.80 in the crystal region. This latter value suggests that the layers have a hexagonal crystal structure (triangular symmetry) with, however, some defects.

In-plane 2D positional $g(\mathbf{r})$ and orientational $G_6(\mathbf{r})$ pair correlation functions for the confined layers at two different temperatures are presented in figures 6 and 7, respectively. Correlations within each layer were

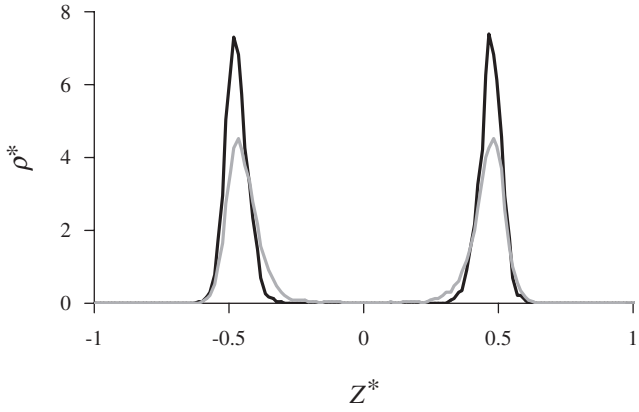

Figure 4. Density profiles in reduced units $\rho^* = \rho\sigma^3_{Ar}$ of Ar/CH_4 mixture with $x_{CH4} \sim 0.9$ confined in a slit graphite pore with $H = 3\sigma_{Ar}$: $T^* = 1.14$ (black line) and $T^* = 1.36$ (grey line). Temperatures are reduced with respect to ε_{Ar}. Z^* is the distance from the pore center in reduced units with respect to σ_{Ar}.

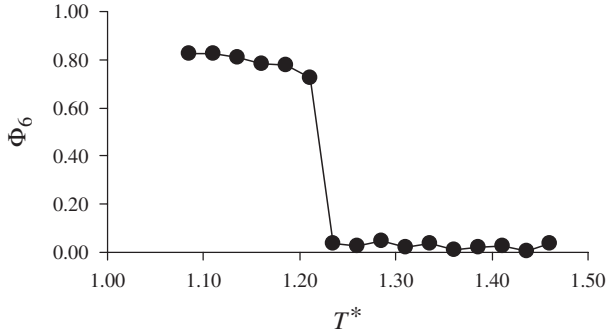

Figure 5. Average value of the 2D bond-order parameter Φ_6 as a function of the reduced temperature T^* for an Ar/CH_4 mixture confined in a $H = 3\sigma_{Ar}$ slit graphite pore.

determined up to a distance of half the size of the simulation box. At $T^* = 1.31$, the confined layers exhibit a liquid-like behavior as revealed by the g(**r**) function, which is characteristic of a phase having short-range positional order. This result is confirmed by the exponential decay observed in the G_6(**r**) function; such a decay is typical of 2D liquid phases, which have short-range orientational order. At $T^* = 1.11$, the confined layers appear as 2D hexagonal crystals with long-range positional order as can be seen from the features of the g(**r**) function for this temperature; (i) the amplitude between the first and the second peak is close to 0, (ii) the second peak is split into two secondary peaks, and (iii) the third peak presents a shoulder on its right

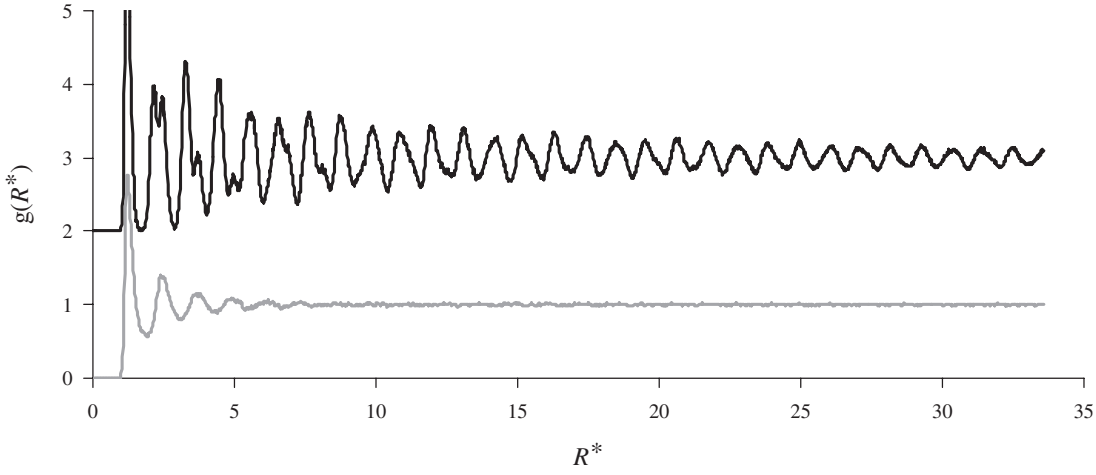

Figure 6. In plane 2D positional pair correlation function g(R^*) for an Ar/CH_4 mixture confined in a $H^* = 3\sigma_{Ar}$ slit graphite pore: $T^* = 1.11$ (black line) and $T^* = 1.31$ (grey line). Temperatures are reduced with respect to ε_{Ar}. The g(R^*) for $T^* = 1.11$ has been shifted by +2.0 for the sake of clarity. R^* is the distance in reduced units with respect to σ_{Ar}.

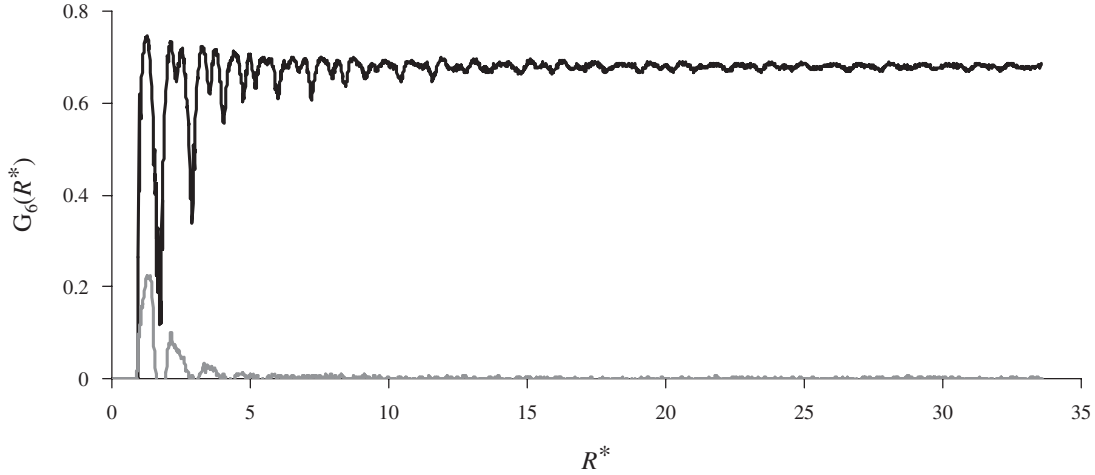

Figure 7. In plane 2D bond-orientational pair correlation function $G_6(R^*)$ for an Ar/CH_4 mixture confined in a $H = 3\sigma_{Ar}$ slit graphite pore: $T^* = 1.11$ (black line) and $T^* = 1.31$ (grey line). Temperatures are reduced with respect to ε_{Ar}. R^* is the distance in reduced units with respect to σ_{Ar}.

side. Moreover, the $G_6(\mathbf{r})$ function at this temperature has a constant average value as expected for a hexagonal crystal layer with long-range orientational order. Analysis of the in-plane 2D pair correlation functions $g(\mathbf{r})$ and $G_6(\mathbf{r})$ corroborate the results shown in figure 5 for the 2D bond-order parameter Φ_6; the transition temperature between the crystal and liquid phases was found to be $T^* = 1.22 \pm 0.02$. For all molar compositions studied in this work, it seems that freezing of the confined layers involves a direct phase transition between a 2D-crystal and a 2D-liquid. This result departs from previous molecular simulation and experimental works for pure substances in which the existence of a hexatic phase between the crystal and liquid phases was reported [54, 55]. Such an intermediate phase is expected according to the theory by Kosterlitz–Thouless–Halperin–Nelson–Young for the melting of 2D systems [47, 48, 56, 57]. The stability of the hexatic phase depends on the size of the system, so that the existence of such an intermediate phase cannot be ruled out or confirmed in the present work unless a scaling size analysis is performed [54].

The CH_4 mole fraction of the Ar/CH_4 confined mixture in equilibrium with a bulk mixture, $x_{CH_4}^{bulk} = 0.5$ is shown as a function of the temperature in figure 8. Upon freezing, the CH_4 mole fraction sharply increases at $T_f^* = 1.22$ from $x_{CH_4}^L = 0.85$ in the liquid phase up to $x_{CH_4}^C = 0.87$ in the solid phase. This analysis provides a first set of crystal/liquid coexistence conditions $(T_f^*, x_{CH_4}^L, x_{CH_4}^C)$ (see table 2). The freezing temperature for the confined mixture, $T_f^* = 1.22$, is much larger than the freezing point of a bulk mixture having the same molar composition, $T_f^{*,bulk} \sim 0.81$, and corresponds to a relative increase of ~ 1.5. The sharp increases observed in the 2D bond-order parameter Φ_6 (figure 5) and the CH_4 mole fraction (figure 8) suggest that the freezing of the confined layers is a first-order transition; however, free energy calculations are required to confirm in a rigorous way the nature of the liquid to crystal transition. Thanks to the use of the parallel tempering technique in which both the liquid and crystal phases are simulated in the same run, we did not perform calculations for the melting process. In our previous work [7], it has been shown that simulations of melting and freezing phenomena give similar results, provided that the parallel tempering method is used and a significant fraction of the swap trial moves are accepted [36, 37]. Moreover, Hung *et al.* [41] showed for pure fluids that this technique gives the same results as those obtained from free energy calculations.

In order to obtain the solid/liquid phase diagram for the confined mixture, we performed simulations for different molar compositions of the bulk mixture (see table 2). For each run, the liquid/solid coexistence

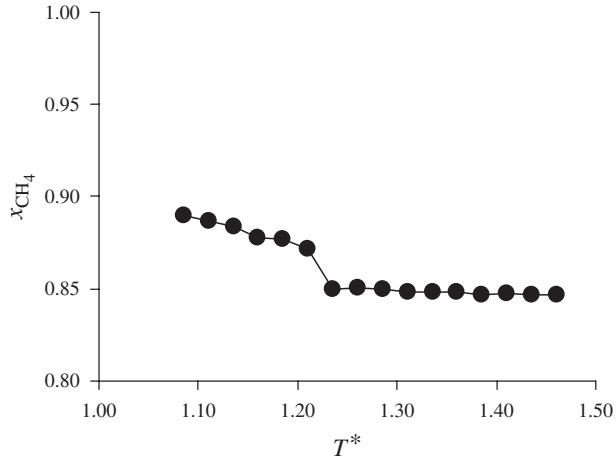

Figure 8. CH_4 mole fraction for an Ar/CH_4 mixture confined in a $H = 3\sigma_{Ar}$ slit graphite pore as a function of the reduced temperature T^* (with respect to ε_{Ar}).

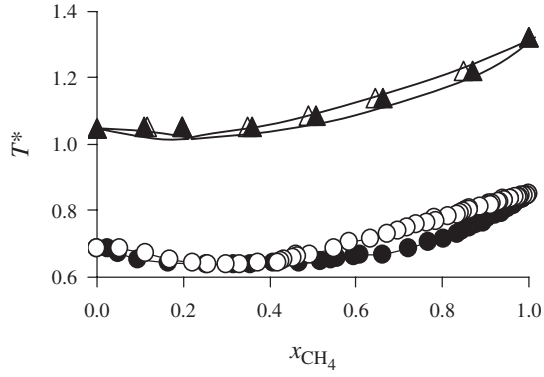

Figure 9. Solid/liquid phase diagram (T^*, x_{CH_4}) at constant reduced pressure $P^* = 0.002$ ($\sim$1 atm) for Ar/CH_4: (circles) are for the bulk mixture, and (triangles) are for the mixture confined in a $H = 3\sigma_{Ar}$ slit graphite pore. Temperatures and pressure are reduced with respect to σ_{Ar} and ε_{Ar}. Open and closed symbols denote the liquid and solid coexistence lines, respectively. The lines between the symbols are provided as a guide to the eye.

$(T_f^*, x_{CH_4}^L, x_{CH_4}^C)$ were determined following the analysis described above; freezing was monitored through the changes of x_{CH_4} and Φ_6 with temperature, and the structure of the confined mixture was studied using both in-plane 2D positional $g(\mathbf{r})$ and bond-orientational $G_6(\mathbf{r})$ pair correlation functions. The coexistence data for each run are reported in table 2. The solid/liquid phase diagram for the Ar/CH_4 mixture confined in the $H^* = 3$ slit graphite pore is shown in figure 9. We also report the phase diagram for the bulk mixture, which was calculated using the Gibbs–Duhem integration technique (see section 2.2.1). The phase diagram for the confined mixture is of the same type, i.e. azeotropic, as that for the bulk system, but the liquid and crystal

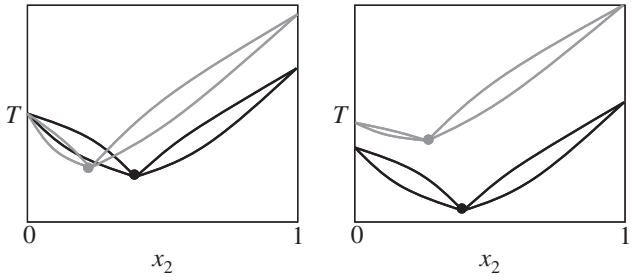

Figure 10. (*Left*) Schematic solid/liquid phase diagrams corresponding to bulk azeotrope binary mixtures for which component 2 has a higher freezing temperature than component 1 (black line). The azeotrope arises from the coexistence line originating from pure component 2 that crosses the freezing temperature of pure component 1 (Grey line). The location of the azeotrope is shifted towards the component having the weakest fluid/fluid interaction (component 1) if the freezing temperature of component 2 is increased. (*Right*) Schematic comparison between the azeotrope phase diagram for a bulk mixture (black line) and that for a confined mixture (grey line). Component 2 has a larger α parameter so that the increase in the freezing temperature compared to the bulk is larger for this component than that for component 1. As a result, the coexistence lines that originate from confined pure component 2 reaches the freezing temperature of confined pure component 1 at a lower value of x_2 compared to the bulk. Consequently, the azeotrope for the confined mixture is shifted to a lower x_2 mole fraction than the bulk.

coexistence lines are located at higher temperatures. We note that we obtained similar results in our previous work on the freezing of mixtures having an ideal solution phase diagram [7, 8]. As in the case of the experiments described in the previous section, the larger freezing temperature for the confined mixture compared with the bulk can be explained by the fact that the wall/fluid interactions are stronger than the fluid/fluid interactions for both Ar and CH_4, i.e. $\alpha_{Ar} > 1$ and $\alpha_{CH_4} > 1$. The slightly smaller increase in the freezing temperature for Ar, $T_f^*/T_f^{*,\mathrm{bulk}} = 1.52$, compared with that for CH_4, $T_f^*/T_f^{*,\mathrm{bulk}} = 1.56$, is consistent with the fact that α_{Ar} is slightly lower than α_{CH_4} (see table 1).

The azeotrope for the confined mixture is located at a CH_4 mole fraction $x^0_{CH_4} = 0.20$ and a temperature $T^{*,0} = 1.0$; the crystal phase for $x_{CH_4} < x^0_{CH_4}$ is richer in Ar than the liquid phase, while the crystal phase for $x_{CH_4} > x^0_{CH_4}$ is richer in CH_4 than the liquid phase. This situation is similar to that observed for the bulk where freezing involves an increase in x_{CH_4} for mole fractions above the azeotrope composition and a decrease in x_{CH_4} for mole fractions below the azeotrope composition. The azeotrope for the confined mixture, $x^0_{CH_4} = 0.20$, is located at a CH_4 mole fraction lower than that for the bulk mixture, $x^{\mathrm{bulk},0}_{CH_4} = 0.30$. Such a result can be qualitatively explained as follows (see figure 10). We know from previous works on bulk mixtures (see, for instance [13, 14]) that an azeotrope appears when the coexistence line that originates from pure component 2 (having the strongest fluid/fluid interaction and therefore the highest freezing temperature) reaches the freezing temperature of component 1 (having the weakest fluid/fluid interaction and therefore the lowest freezing temperature). It is observed that the location of the azeotrope is shifted towards the component having the weakest fluid/fluid interaction (component 1) if the freezing temperature of component 2 is increased (see figure 10). Let us now consider the case of a confined mixture. We assume that component 2 has a larger α parameter than component 1 so that the increase in the freezing temperature is larger for component 2 than that for component 1. As a result, the coexistence lines that originate from confined pure component 2 reaches the freezing temperature of confined pure component 1 at a lower value of x_2 than the bulk. Consequently, the azeotrope for the confined mixture is shifted towards the low x_2 mole fractions with respect to the bulk (see figure 10). Such a reasoning qualitatively explains the shift in the location of the azeotrope between the bulk and the confined mixtures in our molecular simulations (given that $\alpha_{Ar} < \alpha_{CH_4}$, Ar and CH_4 correspond to components 1 and 2, respectively). We cannot check this reasoning in the case of the experiments since, as previously noted, the exact mole fraction within the pore is not known (see section 3.1).

The simulations for Ar/CH_4 mixtures confined in slit graphite pores are in general agreement with the experiments for CCl_4/C_6H_{12} confined in ACF. In both series of results, we observe that the phase diagram for the confined mixture is of the same type as that for bulk mixture, i.e. azeotropic. On the other hand, the solid and liquid coexistence lines are located at larger temperatures. The larger increases in the freezing temperatures in the case of the simulations, $T_f^*/T_f^{*,\mathrm{bulk}} \sim 1.5$–$1.6$, compared to the experiments, $T_f^*/T_f^{*,\mathrm{bulk}} \sim 1.1$–$1.2$, can be explained by the larger values of the α parameters for the mixtures considered in the simulations.

4. Conclusion

We have described experiments and molecular simulations of the freezing of azeotropic mixtures confined in nanoporous carbons. Dielectric relaxation experiments were used to determine the solid/liquid phase diagram of CCl_4/C_6H_{12} mixtures in activated carbon fibres. Grand Canonical Monte Carlo simulations combined with the parallel tempering technique were used to study freezing of the azeotropic Lennard–Jones mixture Ar/CH_4 in a graphite slit pore. Simulations and experiments are in qualitative agreement. Both series of results show that

the phase diagram of the confined mixture is of the same type as that for the bulk. The solid/liquid coexistence lines for the confined system are located at higher temperatures than those for the bulk. GCMC simulations show that the azeotrope is shifted, upon confinement, towards the component having the largest ratio of the wall/fluid to fluid/fluid interactions. It was not possible to verify such a trend in the case of the experiments because of the lack of knowledge of the molar composition within the pore (only the global mole fraction bulk + confined mixtures is known).

Further experiments and molecular simulations are needed to corroborate our results. Differential scanning calorimetry should confirm the transition temperatures found in this study. X-ray diffraction or neutron scattering would allow us to determine the structure of the confined phases. Although the use of the parallel tempering technique greatly reduces the risk of being trapped in a metastable state, we plan to combine the present simulations with free energy calculations to corroborate our findings. In future work we will also consider the effect of confinement by repeating our experiments and molecular simulations for different pore sizes. We will also address the effect of the wall/fluid interaction by considering different nanoporous materials, such as silica adsorbents (controlled pore glass, Vycor, MCM-41, or SBA-15).

Acknowledgements

We are grateful to Henry Bock and Erik Santiso (North Carolina State University) for helpful discussions and comments. This work was supported by the Petroleum Research Fund of the American Chemical Society and by the Polish Science Foundation (*Komitet Badan Naukowych*). Supercomputing time was provided by the National Partnership for Advanced Computational Infrastructure (NSF/NRAC – MCA93SO11) and the National Energy Research Scientific Computing Center (DOE – DE-FGO2–98ER14847). International cooperation was supported by a NATO Collaborative Linkage Grant (No. PST.CLG.978802).

References

[1] L.D. Gelb, K.E. Gubbins, R. Radhakrishnan, M. Sliwinska-Bartkowiak. *Rev. Prog. Phys.*, **62**, 1573 (1999).
[2] H.K. Christenson. *J. Phys.: Condens. Matter*., **13**, 95 (2001).
[3] C. Alba-Simionesco, B. Coasne, G. Dosseh, G. Dudziak, K.E. Gubbins, R. Radhakrishnan, M. Sliwinska-Bartkowiak. *J. Phys.: Condens. Matter*, submitted (2005).
[4] R.R. Meyer, J. Sloan, R.E. Dunin-Borkowski, A.I. Kirkland, M.C. Novotny, S.R. Bailey, J.L. Hutchison, M.L.H. Green. *Science*, **289**, 1324 (2000).
[5] M. Wilson. *J. chem. Phys*., **116**, 3027 (2002).
[6] B. Cui, B. Lin, S. Rice. *J. chem. Phys*., **119**, 2386 (2003).
[7] B. Coasne, J. Czwartos, K.E. Gubbins, F.R. Hung, M. Sliwinska-Bartkowiak. *Mol. Phys*., **102**, 2149 (2004).
[8] B. Coasne, J. Czwartos, K.E. Gubbins, F.R. Hung, M. Sliwinska-Bartkowiak. *Adsorption*, **11**, 301 (2005).
[9] R. Radhakrishnan, K.E. Gubbins, M. Sliwinska-Bartkowiak. *J. chem. Phys*., **116**, 1147 (2002).
[10] D.A. Kofke. *Mol. Phys*., **78**, 1331 (1993).
[11] D.A. Kofke. *J. chem. Phys*., **98**, 4149 (1993).
[12] D.A. Kofke. In *Monte Carlo Methods in Chemistry*, D.M. Ferguson, J.I. Siepmann, D.G. Truhlar (Eds), Interscience, New York (1998).
[13] M.R. Hitchcock. Thesis, Monte Carlo simulations of complete phase equilibria for binary mixtures, North Carolina State University (2000).
[14] M.R. Hitchcock, C.K. Hall, *J. chem. Phys*., **110**, 11433 (1999).
[15] D. Nicholson, N.G. Parsonage. *Computer Simulation and the Statistical Mechanics of Adsorption*, Academic Press, London (1982).
[16] M.P. Allen, D.J. Tildesley. *Computer Simulation of Liquids*, Clarendon Press, Oxford (1987).
[17] D. Frenkel, B. Smit. *Understanding Molecular Simulation*, 2nd edn., Academic Press, New York (2002).
[18] R. Radhakrishnan, K.E. Gubbins, M. Sliwinska-Bartkowiak. *J. chem. Phys*., **112**, 11048, (2000).
[19] B. Widom. *J. chem. Phys*., **39**, 2802 (1963).
[20] B. Widom. *J. stat. Phys*., **85**, 563 (1978).
[21] B. Widom. *Physica A*, **168**, 149 (1990).
[22] B. Widom. *Physica A*, **194**, 532 (1993).
[23] B. Widom. *J. phys. Chem*., **9**, 2803 (1995).
[24] A.E. Van Giessen, D.J. Bukman, B. Widom. *J. coll. Interface Sci*., **192**, 257 (1997).
[25] A.B. Kolomeisky, B. Widom. *Faraday Discuss*., **112**, 81 (1999).
[26] K. Kaneko, A. Watanabe, T. Iiyama, R. Radhakrishnan, K.E. Gubbins. *J. phys. Chem*. B, **103**, 7061 (1999).
[27] M. Sliwinska-Bartkowiak, J. Gras, R. Sikorski, R. Radhakrishnan, L.D. Gelb, K.E. Gubbins. *Langmuir*, **15**, 6060 (1999).
[28] A. Chelkowski. *Dielectric Physics*, Elsevier, New York (1980).
[29] M.H. Lamm, C.K. Hall. *Fluid Phase Equilibria*, **182**, 37 (2001).
[30] M.H. Lamm, C.K. Hall. *AIChE J*., **47**, 1664 (2001).
[31] M.H. Lamm, C.K. Hall. *Fluid Phase Equilibria*, **194–197**, 197 (2002).
[32] M. Mehta, D.A. Kofke. *Chem. Eng. Sci*., **49**, 2633 (1994).
[33] W.B. Streett, L.A.K. Staveley. *J. chem. Phys*., **47**, 2449 (1967).
[34] J.S. Rowlinson. *Liquids and Liquid Mixtures*, Butterworth Scientific, London (1982).
[35] R.F. Cracknell, D. Nicholson, N. Quirke. *Mol. Phys*., **80**, 885 (1993).
[36] Q.L. Yan, J.J. de Pablo. *J. chem. Phys*., **111**, 9509 (1999).
[37] R. Faller, Q.L. Yan, J.J. de Pablo. *J. chem. Phys*., **116**, 5419 (2002).
[38] E. Marinari, G. Parisi. *Europhys. Lett*., **191**, 451 (1992).

[39] Q.L. Yan, J.J. de Pablo. *J. chem. Phys.*, **113**, 1276 (2000).
[40] M. Sliwinska-Bartkowiak, F.R. Hung, E.E. Santiso, B. Coasne, G. Dudziak, F.R. Siperstein, K.E. Gubbins. *Adsorption*, **11**, 391 (2005).
[41] F.R. Hung, B. Coasne, K.E. Gubbins, E.E. Santiso, F.R. Siperstein, M. Sliwinska-Bartkowiak. *J. chem. Phys.*, **122**, 144706 (2005).
[42] W.A. Steele. *Surf. Sci.*, **36**, 317 (1973).
[43] W.A. Steele. *The Interaction of Gases with Solid Surfaces*, Pergamon Press, Oxford (1974).
[44] J.K. Johnson, J.A. Zollweg, K.E. Gubbins. *Mol. Phys.*, **78**, 591 (1993).
[45] R. Radhakrishnan, K.E. Gubbins. *Mol. Phys.*, **96**, 1249 (1999).
[46] F.R. Hung, G. Dudziak, M. Sliwinska-Bartkowiak, K.E. Gubbins. *Mol. Phys.*, **102**, 223 (2004).
[47] B.I. Halperin, D.R. Nelson. *Phys. Rev. Lett.*, **41**, 121 (1978); D.R. Nelson, B.I. Halperin. *Phys. Rev.* B, **19**, 2457 (1979); A.P. Young, *Phys. Rev.* B, **19**, 1855 (1979).
[48] K.J. Strandburg. *Rev. Mod. Phys.*, **60**, 161 (1988).
[49] M. Miyahara, K.E. Gubbins. *J. chem. Phys.*, **106**, 2865 (1997).
[50] A. Tkatchenko, Y. Rabin. *Solid State Commun.*, **103**, 361 (1997).
[51] A. Tkatchenko, Y. Rabin. *Langmuir*, **13**, 7146 (1997).
[52] A. Weinstein, S. Safran. *Europhys. Lett.*, **42**, 61 (1998).
[53] Z. Tan, K.E. Gubbins. *J. phys. Chem.*, **96**, 845 (1992).
[54] R. Radhakrishnan, K.E. Gubbins, M. Sliwinska-Bartkowiak. *Phys. Rev. Lett.*, **89**, 076101 (2002).
[55] R. Radhakrishnan, K.E. Gubbins, M. Sliwinska-Bartkowiak. *Phys. Rev.* B, submitted (2005).
[56] J.M. Kosterlitz, D.J. Thouless. *J. phys.* C, **5**, L124 (1972).
[57] J.M. Kosterlitz. D.J. Thouless. *J. phys.* C, **6**, 1181 (1973).